

# Hybrid improper ferroelectricity in a Multiferroic and Magnetoelectric hybrid organic-inorganic perovskite

Alessandro Stroppa,<sup>1</sup> Paolo Barone,<sup>1</sup> Prashant Jain,<sup>2</sup> Jean Manuel Perez-Mato,<sup>3</sup> and Silvia Picozzi<sup>1</sup>

<sup>1</sup>*CNR-SPIN, L'Aquila, Italy*

<sup>2</sup>*Los Alamos National Lab, 30 Bikini Atoll Rd Los Alamos, NM 87545-0001 (505) 664-5265*

<sup>3</sup>*Departamento de Fisica de la Materia Condensada, Facultad de Ciencia y Tecnologia, UPV/EHU, Bilbao (Spain)*

There is great interest in hybrid organic-inorganic materials such as metal-organic frameworks (MOFs). The compounds  $[\text{C}(\text{NH}_2)_3]\text{M}(\text{HCOO})_3$ , where  $\text{M}=\text{Cu}^{2+}$  or  $\text{Cr}^{2+}$  are Jahn-Teller (JT) active ions, are MOF with perovskite topology which crystallizes in polar space group  $\text{Pna}2_1$ . In inorganic compounds, octahedral tilting and Jahn-Teller structural distortions are usually non-polar distortions. However, in this MOF cooperative interactions between the antiferro-distortive distortions of the framework and the  $\text{C}(\text{NH}_2)_3$  organic cation via hydrogen bonding breaks the inversion symmetry and induces a ferroelectric polarization. [Angew. Chem. Int. Ed. **50**, 5847, 2011] Our ab-initio study supports the picture of an orbital-order-induced ferroelectricity, a rare example of dipolar ordering caused by electronic degrees of freedom. Moreover, the switching of polarization direction implies the reversal of the weak ferromagnetic component. The microscopic mechanism of the multiferroicity and magnetoelectric coupling in this JT-based MOF with  $\text{ABX}_3$  perovskite structure displays a Hybrid Improper Ferroelectric (HIF) state, arising from a trilinear coupling between different structural deformations that comprise tilting, rotations and Jahn-Teller distortions of both the  $\text{BX}_3$  framework and the organic cation at the A sites. Since these distortion modes in perovskite-inorganic compounds usually freeze-in at elevated temperatures, the trilinear coupling in MOF compounds may provide an interesting route towards high-temperature multiferroicity. These results therefore offer an important starting point for tailoring multiferroic properties in this emerging class of materials for various technological applications. In particular, the high tunability of the ferroelectric polarization by means of the modification of the organic A cation has been recently shown [J. Am. Chem. Soc. **135** 18126 (2013)]

Email: alessandro.stroppa@spin.cnr.it

Keywords: Hybrid organic-inorganic perovskite, Metal-Organic Frameworks, Hybrid Improper Ferroelectricity, Multiferroic, Magnetoelectric

Metal-organic frameworks (MOFs) are hybrid crystalline compounds comprised of extended ordered networks formed from organic linkers and metal cations, often forming porous materials at the interface of molecular coordination chemistry and materials science. They show unique properties arising from organic-inorganic duality[1] which has already resulted in an unprecedented variety of physical properties in a single class of materials and applications, such as gas storage, exchange or separation, catalysis, drug delivery, optics, and magnetism.[2, 3] An additional feature is the possibility of creating ideally infinite new MOFs by varying inorganic/organic components, molecular topologies, organic linkers, etc.[5–11] All these degree of freedoms can be exploited for a rational design of new materials with enhanced functionalities.

MOFs with  $\text{ABX}_3$  perovskite structure or closely related superstructures of this chemical *chameleon* have attracted much attention since they show promising properties in areas that have traditionally been dominated by inorganic materials, for example magnetism and ferroelectricity.[12–15] Combination of spontaneous magnetic and ferroelectric order in a single material, *i.e.* multiferroicity (MF), is of great technological and fundamental importance, in particular when both orders are coupled through a sizeable magneto-electric coupling (ME). Despite the large activity devoted to multiferroics,[16] most of the past and current studies have been focused on inorganic compounds, though mainly in the family of perovskite-like oxides. Among these, a strong ME coupling is expected in magnetically driven improper ferroelectrics, such as rare-earth manganites or delafossite oxides, where the magnetic ordering is responsible for spontaneous electric polarization.[17] Unfortunately, the symmetry-breaking is usually associated with frustrated magnetism displaying antiferromagnetic or spiral order, and both measured electric polarization and critical temperatures are usually too small for any device applications.[17] The large ferroelectric polarization of proper multiferroics such as  $\text{BiFeO}_3$ , on the other hand, originates from a polar lattice instability that is generally not coupled to any magnetic instability leading to a net magnetization.[18]

Very recently, a third class of magnetoelectric multiferroics has been suggested, where a lattice instability is responsible for both ferroelectricity and the appearance of a weak-ferromagnetic (WFM) ordering, thus allowing for a potentially large ME coupling. The key ingredient is a trilinear coupling between a (stable) polar mode and two

nonpolar instabilities, usually octahedron tilting and rotations in layered or double perovskites, as recently found in some inorganic compounds, where layered cation ordering leads to the required symmetry breaking.[19, 20, 22–24] The mechanism has been called “hybrid improper ferroelectricity”, alluding to the fact that polarization appears as a secondary order parameter from the trilinear coupling to non-polar unstable modes.[20] Remarkably, the experimental evidence of the proposed mechanism in a class of inorganic compounds has been recently put forward.[21]

Here, we theoretically predict that a Cr based MOF (hereafter called Cr-MOF) of  $ABX_3$  perovskite topology  $[C(NH_2)_3]M[(HCOO)_3]$ , not yet synthesized,[25] should be a new multiferroic and we predict a *very large* WFM component which is coupled to ferroelectricity. We will show that it belongs to the class of “hybrid improper” multiferroics.[20] Specifically, we found that the rotational mode associated to A-site molecules and the Jahn-Teller (JT) distortions of the  $Cr^{2+}$  ions are unstable primary modes while the polar mode is soft but stable. The ferroelectricity arises only because the stable polar mode is coupled to the two nonpolar unstable modes, through a trilinear coupling. Microscopically, this coupling is expected to be mediated by hydrogen bondings connecting the guanidinium cations with the distorted metal framework, as discussed in Ref.[26]. Here, for the first time, the “hybrid improper” nature of ferroelectricity involving JT modes is found and discussed in a MOF with  $ABX_3$  structure. Furthermore, we propose a microscopic model showing that the WFM originates from the peculiar magnetic anisotropy of JT ions in combination with the strongly distorted structure of the metal framework.[27] Our theoretical predictions point therefore to a central role of Jahn-Teller interaction in driving both FE and ME properties. Finally, we predict by means of Monte Carlo calculations a critical temperature  $T_c \sim 40$  K for the WFM phase, one of the largest among the class of the  $ABX_3$  MOF compounds.[28, 29]

A new family of MOFs in perovskite  $ABX_3$  topology has been synthesized,[25] such as  $[C(NH_2)_3]M[(HCOO)_3]$ , where  $A=C(NH_2)_3^+$  is the guanidinium cation,  $M^{+2}$  is a divalent metal atom (Mn, Fe, Co, Ni, Cu or Zn) and X is the formate  $HCOO^-$ . The Cu based MOF, which is the only one of the series containing a JT ion, crystallizes in a polar space group,  $Pna2_1$ , displaying both ferroelectricity and WFM, while all the others are isostructural and crystallize in a non-polar  $Pnna$  space group.[25, 26]

Here we combined density functional theory calculation, symmetry analysis and model Hamiltonian in order to investigate the case of the JT active  $Cr^{+2}$  ion. Although it may be difficult to stabilize the Cr ion in a low oxidation state  $+2$ , very recently the homologous inorganic compound  $K^+Cr^{+2}F^{-1}_3$  has been synthesized and studied over a wide range of temperature.[30] The top and side view of the Cr-MOF are shown respectively in Fig. 1 (a) and (b), while in Fig. 1 (c) the A-group guanidinium is shown. Starting from the crystal structure of the Cu-MOF, we replaced the  $Cu^{+2}$  ( $t_{2g}^6e_g^3$ , twofold hole degeneracy) ions by  $Cr^{+2}$  active ions ( $t_{2g}^3e_g^1$ , twofold electron degeneracy). In both cases, they are JT active. For  $Cr^{+2}$ , as a result of strong Hund’s rule coupling, spin of the  $e_g$  electron is parallel to spins of the  $t_{2g}$  electrons on same site. The relaxed polar crystal structure  $Pna2_1$  turns out to be more stable than the centric  $Pnna$  space group by about  $\sim 0.08$  eV/formula unit. The  $CrX_6$  octahedra (X=HCOO) are strongly axially distorted, comprising *medium* Cr-X bonds  $\sim 2.033$  Å along  $c$  axis, and alternating *long* 2.358 Å and *short* 2.010 Å in  $ab$  plane. Orientation of long Cr-X bonds in  $ab$  plane is a direct result of the cooperative Jahn-Teller distortions (CJTDs) resulting in antiferrodistortive pattern of long and short bonds in  $ab$  plane: long bonds form two ferrodistortive sublattices characterized by a parallel orientation, however the orientation is rotated by  $\sim 90^\circ$  from one sublattice to another. Such an ordering of long bonds is compatible with an antiferrodistortive ordering of the  $3d_{3x^2-r^2}$  and  $3d_{3y^2-r^2}$  orbitals (OO) in same plane. The orbital pattern is the same when moving along the  $c$  axis. Each octahedron is tilted with respect to the  $c$  axis by  $\sim 31^\circ$ .

In Fig. 2 (a) we report the variation of total energy as a function of normalized amplitude  $\lambda$  of the structural distortion connecting the centric  $Pnna$  phase ( $\lambda=0$ ) to polar one ( $\lambda=\pm 1$ ). The expected double-well profile is characteristic of a switchable ferroelectric system.[33] The electric polarization as a function of  $\lambda$  is shown in Fig. 2 (b), displaying a value  $0.22 \mu C/cm^2$  in the most stable structure ( $\lambda=\pm 1$ ). In Fig. 2 (c), we show changes of the antiferrodistortive pattern from centrosymmetric to the polar phase by introducing the Jahn-Teller coordinate vector with components  $Q_2$  and  $Q_3$ , where  $Q_2 = (l - s)/\sqrt{2}$  and  $Q_3 = (2m - l - s)/\sqrt{6}$ :[31, 32] here  $l$  and  $s$  refer to lengths of the long and short bonds, respectively, in  $ab$  planes and  $m$  to the lengths of  $CuO_{ap}$  bonds and the JT phase is defined as  $\phi = \tan^{-1} Q_2/Q_3$ . Due to the JT effect, degeneracy of the  $e_g$  orbitals is lifted and the occupied orbital is defined as  $|\theta\rangle = \cos\frac{\phi}{2}|3z^2 - 1\rangle + \sin\frac{\phi}{2}|x^2 - y^2\rangle$ . One can monitor the antiferro-distortive pattern via changes in  $\phi$ . For  $\lambda = 1$  (positive polarization),  $\phi$  is  $\sim 4\pi/3$  for the octahedra elongated along  $[1,1,0]$  and  $2\pi/3$  for octahedra elongated along  $[\bar{1},1,0]$ . For  $\lambda = -1$  (negative polarization), the Jahn-Teller phase is swapped between the two octahedral sublattices, *i.e.* the direction of the elongated axes are interchanged [see Fig.2 (c)], while the antiferro-distortive pattern disappears for  $\lambda = 0$  (centrosymmetric) phase, *i.e.*  $\phi = \pi$ ,  $Q_2 = 0$  and  $l = s$ . It is remarkable to note the correlated behavior of  $\phi$  and that of the polarization, as a function of  $\lambda$ . This is confirmed by a fit testing procedure using  $P(\lambda) = A_0 \tan(A_1 \lambda)$  in Fig.2 (b), which shows a very good agreement between the data-points calculated by using modern theory of polarization and the data-points calculated with the proposed fitting function. Note that by definition, the JT  $\phi$  phase has the same functional behaviour. The spin-polarized charge density of the  $e_g$  electron is also shown in the inset of Fig. 2 (c), showing that the ferroelectric order, the AFD JT distortions and the related orbital

order are clearly correlated. It is important to note that in standard perovskite  $ABX_3$  compounds antiferrodistortions are never associated to a polar behavior.[34]

The magnetic structure of the Cr-MOF is strongly influenced by the antiferrodistortive JT distortions. The orbital ordering induced by the CJTDs effectively confines the magnetic interactions to linear chains along the  $c$  axis[35, 36]. In agreement with Goodenough-Kanamori rules, the super-exchange interaction  $J_c$  along the  $c$  axis is antiferromagnetic and larger than the ferromagnetic exchange interaction  $J_{ab}$  in the  $ab$  planes, due to the orthogonality of the JT magnetic orbitals; as a result, the ground state displays an A-type antiferromagnetic (AFM-A) configuration (see Table S1 in supplemental material). From total-energy calculations and assuming  $S = 2$  spins for Cr ions, we estimate the exchange couplings as  $J_c \simeq 0.823 \text{ meV}$  and  $J_{ab} \simeq -0.452 \text{ meV}$ , confirming strong anisotropies of magnetic exchanges. According to our *ab-initio* calculations, the spins deviate from the collinear arrangement giving rise to a WFM component along the crystallographic  $c$  axis as large as  $\sim 1 \mu_B$ . This ferromagnetic component is clearly correlated with the ferroelectric polarization, as shown in Fig. 2 (d), *i.e.* the Cr-MOF is expected to be a magnetoelectric compound.

Within the distortion mode connecting the Pnna structure to the Pna21 structure, there can be atomic displacements hybridized with true polar modes which do not contribute to the electric polarization, as it happens here with the JT distortion. In order to check this, it is useful to introduce a higher supergroup for describing possible distortion modes and separate their role in the polar behavior. In our case, the Pnna is pseudosymmetric with respect to a higher symmetry Imma space group. It is therefore possible to describe the polar structure with respect to this centric Imma structure. The global distortion relating the Imma and the Pna21 can be decomposed into three distinct atomic distortions: two zone-boundary modes at the  $X$  point, transforming as the irreducible representations  $X_{1-}$ ,  $X_{4+}$ , and a polar zone-center mode transforming as  $\Gamma_{4-}$ . They lower the symmetry to Pnna, Pnma and Imma2 respectively (isotropy subgroups). Therefore, the first two modes do not produce any polarization since the Pnna and Pnma are non-polar space group, while the only one producing the actual polarization is the  $\Gamma_{4-}$  mode. It is worth noting here that it is possible to reach the Imma2 polar group without the zone-center polar instability, *i.e.* only with a combined distortion  $X_{1-} \oplus X_{4+}$ . [20] The relative size of symmetry-adapted mode amplitudes offers valuable clues to interpret the mechanism giving rise to the electric polarization. The amplitude of these modes  $Q$  is very different: 0.57, 2.87 and 0.16 Å for  $X_{1-}$ ,  $X_{4+}$  and  $\Gamma_{4-}$  respectively. The fact that  $Q_{X_{1-}}$  and  $Q_{X_{4+}}$  are much larger than  $Q_{\Gamma_{4-}}$  suggests that the two first distortion modes are the primary structural distortions with respect to the prototype phase, acting as order parameters, while the polar mode is a secondary induced distortion. To confirm this, we have calculated the variation of the total energy with respect to the Imma structure (taken as zero energy reference) as a function of the amplitude of each individual mode,  $Q_{X_{1-}}$ ,  $Q_{X_{4+}}$ , and  $Q_{\Gamma_{4-}}$ , as shown in Fig. 3.

It is clear that  $\Gamma_{4-}$  mode is stable and very soft, while the  $X_{1-}$  and  $X_{4+}$  are unstable. In the same figure, inset from the left, we also report the subgroup tree relation, which shows the chain of maximal subgroups connecting the Imma and Pna21 space groups. The latter appear as a common maximal subgroup of any pair of the space groups. It can be seen that the intersection of two mentioned isotropy subgroups is the observed Pna21 space group, as it is the largest common subgroup of the Pnna and Pnma space groups. This implies that the combination of these two non-polar modes is able to induce a polar phase (although they do not produce a polarization by themselves).

It is interesting to visualize the distortion modes, when viewed as atomic displacements with respect to the reference Imma structure. In the right part of Fig. 3, we show only the  $X_{1-}$  and  $X_{4+}$  mode. The former shows significant displacements on the A-group molecule, and it represents a rotation around the  $c$  axis which is anticlockwise along the  $a$  axis, and alternating clockwise (counterclockwise) along  $c$  axis. The latter clearly represents the characteristic pattern of distortion of the  $Q_2$  JT modes, which induces by hydrogen bondings[26] other distortions on the A-group molecule, in form of a clock-wise rotation around the  $c$  axis. The  $\Gamma_{4-}$  polar mode is not shown for simplicity, but it acts significantly on the A-group atoms.[26] Further details about the mode visualization can be found in the Supplementary Information.

The presence of the polar distortion with a non-negligible significant amplitude can be explained as an induced effect through symmetry-allowed anharmonic trilinear coupling with the primary non-polar distortion modes described as  $Q_{X_{1-}} Q_{X_{4+}} Q_{\Gamma_{4-}}$ . This simple coupling is sufficient to explain the presence of a non-zero amplitude  $Q_{\Gamma_{4-}} \propto Q_{X_{1-}} Q_{X_{4+}}$  in order to minimize the energy, despite the mode itself being essentially stable. The combined  $X_{4+}$  (JT distortion)  $\oplus X_{1-}$  (rotation of group A) is the “hybrid” distortion  $Q_{X_{41}}$  and it is what drives the system into the polar state. This means that the polarization becomes non-zero only when both the guanidinium rotation and JT distortions condense. Examples of hybrid improper ferroelectrics have been recently found in inorganic material chemistry[20]. However, they show more complicated topology than simple  $ABX_3$  type and involve rotational modes such as tilting and rotations of octahedra. Here, for the first time, the hybrid improper ferroelectricity is found in a metal-organic framework in a simple  $ABX_3$ , and it involves a Jahn-Teller mode and rotational mode acting on the A-site. It is important to highlight that the interaction between ferroelectric distortion and two rotational modes represent an important strategy for strong magnetoelectric coupling, possibly at room temperature, as recently shown for inorganic transition-metal oxides.[37] In MOF perovskite there is the additional advantages of the great tunability offered by

the organic-inorganic duality, and the possibility of considering lead-free compounds, which is certainly an important aspect for environmental concerns.

We have shown in Fig. 2 (d) that there is a correlation between WFM component and the ferroelectric polarization, and therefore with the JT distortions. In fact, i) a rotation of the AFD pattern switches the WFM from  $+M(+P)$  to  $-M(-P)$ ;  $\mathbf{M} = 0$  in the centrosymmetric Pnna reference structure, where the JT-induced antiferrodistortive pattern is zero but the octahedra remain strongly tilted. This suggests that Dzyaloshinskii-Moriya interaction (DMI)  $\mathbf{D} \cdot \mathbf{S}_i \times \mathbf{S}_j$ , [38, 39] usually related to octahedra tilting, may not be the source of WFM in this compound. In fact, due to the AFM-A magnetic ordering, only DMI between spins belonging to different  $ab$  planes is relevant; each octahedron is tilted from  $c$  axis by an angle  $\alpha \sim 31^\circ$ , around  $a$  axis: this implies that the Dzyaloshinskii vector  $\mathbf{D}_c$  is parallel to axis  $a$ , as shown in inset from the left of Fig. 2 (d). By using symmetry analysis (see Supplementary Information) it can be shown that only magnetoelectric trilinear coupling terms  $P_c M_c L_a$  or  $P_c M_a L_c$  are allowed in Cr-MOF, where  $\mathbf{P}, \mathbf{M}, \mathbf{L}$  are ferroelectric, ferromagnetic and antiferromagnetic order parameters respectively; in both cases, the cross product  $\mathbf{S}_i \times \mathbf{S}_j$  is parallel to axis  $b$  and perpendicular to  $\mathbf{D}_c$ , as shown in inset from the right of Fig. 2 (d). Therefore  $\mathbf{D} \cdot \mathbf{S}_i \times \mathbf{S}_j$  is zero, thus ruling out DMI as the source for the canted antiferromagnetism.

Our *ab initio* study suggests a relevant role of JT distortions in combination with spin-orbit coupling (SOC) interaction, for the origin of the canted antiferromagnetism. Indeed, both JT and SOC involve the angular moment of the electronic states [34]; furthermore, SOC is usually responsible for magnetic single-ion anisotropy (MSIA), which has been devised by Moriya as an alternative origin for canted antiferromagnetism when neighboring magnetic sites display different anisotropy axes [27]. A second-order perturbation calculation (see Supplementary Information) shows that MSIA energy has the form  $H_{msia} = E \sum_i [(\mathbf{S}_i \cdot \mathbf{s}_i)^2 - (\mathbf{S}_i \cdot \mathbf{l}_i)^2] + D \sum_i (\mathbf{S}_i \cdot \mathbf{m}_i)^2$ , where  $\mathbf{l}_i, \mathbf{s}_i$  are unit vectors along the long and short bonds in M-octahedron basal plane and  $\mathbf{m}_i$  a unit vector parallel to the M-O<sub>ap</sub> bond (see Fig. ??c), where  $E, D$  are the effective magnetic anisotropy constants. From this expression the interplay between SOC and JT interaction is readily seen, since the MSIA energy explicitly depends on the MO<sub>6</sub> octahedral JT distortions. Therefore the local MSIA contribution is affected by the antiferrodistortive pattern of JT distortions and by the tilted structure of the metal framework, both distortions modifying the direction of anisotropies axes on each octahedron (see Supplementary Information). Assuming classical spins, which is a reasonable approximation for Cr spins, and considering MSIA as a small perturbation on the AFM-A magnetic configuration induced by symmetric exchanges  $J_c, J_{ab}$ , the WFM can be described by a small angle  $\epsilon$  representing the spin canting from the collinear spin axis, *i.e.*  $|\mathbf{M}| = S \sin \epsilon$ . By minimizing the mean-field energy, the angle  $\epsilon$  satisfies equation (see Supplementary Information):

$$\tan 2\epsilon = -\frac{2E \sin \alpha}{2J_c \mp D \cos^2 \alpha}, \quad (1)$$

where  $\alpha$  is the tilting angle of octahedra and the sign  $\mp$  is found for  $L_a, L_c$  realizations of the AFM-A ordering respectively. Eq. (1) shows that WFM appears only when tilting distortions ( $\alpha \neq 0$ ) and JT-induced MSIA, through constant  $E \neq 0$ , are simultaneously present. The WFM component points along  $c$  ( $a$ ) direction for  $L_a$  ( $L_c$ ) respectively, and it is reversed when the antiferrodistortive pattern is rotated by  $90^\circ$  with fixed tilting angle ( $\alpha E \mapsto -\alpha E$ ), in agreement with *ab-initio* results.

Since  $D < J_c$ , WFM is present irrespectively of the ratio  $E/D$  provided  $E$  is nonzero: this explains the MSIA as the origin of the WFM component. Note that the proposed mechanism is compatible with the trilinear coupling previously discussed, putting forward the Jahn-Teller interaction as the main responsible for the coupling between  $P$  and  $M$  and for the predicted ME effect. The classical mean-field approximation predicts that the  $L_a, M_c$  realization of the canted AFM-A state is energetically more stable than the  $L_c, M_a$  configuration, in agreement with DFT results, *i.e.* the WFM points along the  $c$  axis. The MSIA parameters have been estimated from DFT calculations as  $E \simeq 0.745 \text{ meV}$  and  $D \simeq 0.113 \text{ meV}$ ; with these values a set of Monte Carlo calculations has been performed, confirming the mean-field analysis and predicting a critical temperature for the onset of the canted AFM-A at  $T_c \simeq 40 \text{ K}$  (see Fig. ??e).

By using state-of-the-art-*ab-initio* calculations, we theoretically predict that the  $[\text{C}(\text{NH}_2)_3]\text{Cr}(\text{HCOO})_3$  MOF should be a new multiferroic with a magnetoelectric coupling. For the first time in the MOF class of compounds we show a peculiar origin of ferroelectricity, as due to a trilinear coupling of two primary unstable non-polar modes with a secondary stable and polar mode. Moreover, we highlight the important role of the Jahn-Teller antiferrodistortions in both the magnetoelectric and ferroelectric coupling. To support our interpretation we have carried out a symmetry mode analysis as well as we propose a microscopic model based on a perturbative approach. These results support the idea that MOFs show promising new routes for achieving multiferroic properties, an otherwise rare phenomenon in pure inorganic materials. Furthermore, a high tunability of the ferroelectric polarization by means of the modification of the organic A cation has been recently shown in Ref. [50].

## Methods

The calculations have been done by using the VASP package [40, 41] with the Perdew-Burke-Ernzerhof (PBE) GGA functional [42]. The energy cutoff was set to 400 eV and a  $2 \times 4 \times 4$  Monkhorst-Pack grid of  $k$ -points was used. The Berry phase approach [43] was employed to calculate the ferroelectric polarization  $P$ . Test calculations using the

Heyd-Scuseria-Ernzerhof hybrid functional (HSE)[44] and with the Grimme corrections for weak-interactions[45] have been considered: the results are robust with respect to the different computational methods giving us confidence in the reliability of the underlying physical mechanisms. Monte Carlo calculations were performed via standard Metropolis algorithm on a  $28 \times 28 \times 28$  cubic lattice with periodic boundary conditions. Symmetry analysis has been performed using the Bilbao Crystallographic Server[46], in particular using the symmetry software PSEUDOSYMMETRY[47] and AMPLIMODES[48, 49]

#### Acknowledgements

This work has been supported by the European Community's Seventh Framework Programme FP7/2007-2013 under grant agreement No. 203523-BISMUTH. A.S. wishes to thank Prof. I. B. Bersuker for useful insights about JT effect. A.S. acknowledges discussions with Dr. C. Autieri and Prof. E. Pavarini. We acknowledge the CINECA award under the ISCRA initiative, for the availability of high performance computing resources and support. We gratefully acknowledge the very valuable help of Emre Tasci when using the tools of the Bilbao Crystallographic Server for the mode analysis and its visualization.

Received: ((will be filled in by the editorial staff))

Revised: ((will be filled in by the editorial staff))

Published online: ((will be filled in by the editorial staff))

- 
- [1] O. M. Yaghi, M. O'Keeffe, N. Ockwig, H. K. Chae, M. Eddaoudi, J. Kim, *Nature* **2003**, 423, 705.
- [2] G  rard F  rey, A.K. Cheetham, *Science* **1999**, 283, 1125.
- [3] C. N. R. Rao, A. K. Cheetham, A. Thirumurugan, *J. Phys.: Condens. Matter* **2008**, 20, 083202.
- [4] K. Sumida, D. L. Rogow, J. A. Mason, T. M. McDonald, E. D. Bloch, Z. R. Herm, T.-H. Bae, J. R. Long, *Chem. Rev.* **2012**, 112, 724.
- [5] M. J. Rosseinsky, *Nat. Mat.* **2010**, 9, 609;  
M. A. Green *Nat. Mat.* **2010**, 9, 539; 2009 Metal-organic frameworks issue, *Chem. Soc. Rev.* **2009** 38, 1201.
- [6] H. Sato, R. Matsuda, K. Sugimoto, M. Takata, S. Kitagawa, *Nature Mater.* **2010** 9, 661.
- [7] R. Makiura, S. Motoyama, Y. Umemura, H. Yamanaka, O. Sakata, H. Kitagawa, *Nature Materials* **2010** 9 565.
- [8] T. C. Narayan, T. Miyakai, S. Seki, M. Dinca, *J. Am. Chem. Soc.* **2012**, 31, 12932.
- [9] A. U. Ortiz, A. Boutin, A. H. Fuchs, F.-X. Coudert, *Phys. Rev. Lett.* **2012**, 109, 195502.
- [10] B. Assfour, S. Leoni, G. Seigert and I. A. Baburin, *Adv. Mat.* **2011**, 23, 1237.
- [11] C. Bosch-Serrano, J.M. Clemente-Juan, E. Coronado, A. Gaita-Arino, A. Pali  , B. Tsukerblat, *Phys. Rev. B* **86** 024432 (2012).
- [12] R. Ramesh, *Nature*, **2009**, 461 , 1218.
- [13] T. Besara, P. Jain, N. S. Dalal, P. L. Kuhns, A. P. Reyes, H. W. Kroto, A. K. Cheetham, *Proc. Natl. Acad. Sci. U. S. A.* **2011**108, 6828.
- [14] P. Jain, V. Ramachandran, R.J. Clark, H.D. Zhou, B.H. Toby, N.S. Dalal, H.W. Kroto, A.K. Cheetham, *J. Am. Chem. Soc.* **2009**, 131, 13625.
- [15] X. Guan-Cheng, Z. Wen, M. Xiao-Ming, C. Yi-Hong, Z. Li, C. Hong-Ling, W. Zhe-Ming, X. Ren-Gen, *G. Song J. Am. Chem. Soc.*, **2011**, 133 14948.
- [16] N. A. Spaldin, M. Fiebig, *Science* **2005** 309, 391.
- [17] S.-W. Cheong, M. Mostovoy, *Nat. Mater.* **2007**, 6, 13.
- [18] J. Wang, J. B. Neaton, H. Zheng, V. Nagarajan, S. B. Ogale, B. Liu, D. Viehland, V. Vaithyanathan, D. G. Schlom, U. V. Waghmare, N. A. Spaldin, K. M. Rabe, M. Wuttig, R. Ramesh, *Science* **2003**, 299, 1719.
- [19] E. Bousquet, M. Dawber, N. Stucki, C. Lichtensteiger, P. Hermet, S. Gariglio, J.-M. Triscone, Ph. Ghosez *Nature (London)* **2008**, 452, 732.
- [20] N. A. Benedek and C. J. Fennie, *Phys. Rev. Lett.* **2011**, 106, 107204.
- [21] C. Adamo, private communication.
- [22] J. Lopez-Perez, J. Iniguez, *Phys. Rev. B* **2011**, 84, 075121.
- [23] J. M. Rondinelli, C. J. Fennie, *Adv. Mat.* **2012** 24, 1961.
- [24] T. Fukushima, A. Stroppa, S. Picozzi, J. M. Perez-Mato, *Phys. Chem. Chem. Phys.* **2011**, 13, 12186.
- [25] K.-L. Hu, M. Kurmoo, M. Wang, S. Gao, *Chem. Eur.* **2009**, 15, 12050.
- [26] A. Stroppa, P. Jain, P. Barone, M. Marsman, J.M. Perez-Mato, A. K. Cheetham, H. W. Kroto, S. Picozzi, *Angew. Chem. Int. Ed.* **2011**, 123, 5969.
- [27] T. Moriya, *Phys. Rev.* **1969**, 120 , 91.
- [28] L.-S. Long, X.-M. Chen, M.-L. Tong, Z.-G. Sun, Y.-P. Ren, R.-B. Huang, L.-S. Zheng, *J. Chem. Soc., Dalton Trans.* **2001**, 2888.
- [29] M. Kurmoo, H. Kumagai, S. M. Hughes and C. J. Kepert, *Inorg. Chem.* **2003**, 42, 6709.
- [30] S. Margadonna, G. Karotsis, *J. Am. Chem. Soc.* **2006**, 128, 16436.
- [31] G. Matsumoto, *J. Phys. Soc. Jpn.* **1970**, 29, 606.

- [32] J. Kanamori, *J. Appl. Phys.* **1960**, 31, 14S.
- [33] M. E. Lines and A. M. Lines, *Principles and applications of ferroelectrics and related materials*, Clarendon. Press, Oxford **1977**.
- [34] I. Bersuker, *The Jahn-Teller Effect*, Cambridge University Press, Cambridge, **2006**.
- [35] J. B. Goodenough, *Magnetism and Chemical Bond*, Interscience Publ., N.Y.-Lnd., **1963**; D. J. Khomskii, in *Spin Electronics* (Eds: M. Ziese and M.J. Thornton), Springer-Verlag, Berlin Heidelberg **2001**.
- [36] M. Towler, R. Dovesi, V. S. Saunders, *Phys. Rev. B* **1995**, 52, 10150.
- [37] P. Ghosez, J.M. Triscone, *Nat. Mat.* **2011**, 10, 269.
- [38] I. Dzyaloshinsky, *J. Phys. Chem. Sol.* **1958**, 4, 241 .
- [39] T. Moriya, *Phys. Rev. Lett* **1960**, 4, 228.
- [40] G. Kresse and J. Furthmüller, *Phys. Rev. B* **1996**, 54, 11169.
- [41] P. E. Blöchl, *Phys. Rev. B* **1994**, 50, 17953.
- [42] J. P. Perdew, K. Burke, M. Ernzerhof, *Phys. Rev. Lett.* **1996**, 77, 3865.
- [43] R. D. King-Smith, D. Vanderbilt, *Phys. Rev. B* **1993**, 47, 1651.
- [44] J. Heid, G. E. Scuseria, M. Ernzerhof, *J. Chem. Phys.* **2003**, 118, 8207.
- [45] S. Grimme, *J. Comput. Chem.* **2004**, 25, 1463.
- [46] <http://www.cryst.ehu.es/>
- [47] C. Capillas, E.S. Tasci, G. de la Flor, D. Orobengoa, J.M. Perez-Mato and M.I. Aroyo, **2011** *Z. Krist.*, 226, 186.
- [48] D. Orobengoa, C. Capillas, M. I. Aroyo and J.M. Perez-Mato **2009** *J. Appl. Cryst.* A42, 820.
- [49] J.M. Perez-Mato, D. Orobengoa and M.I. Aroyo, *Acta Cryst A* **2010** 66 558.
- [50] D. Di Sante, A. Stroppa, P. Jain, S. Picozzi, *J. Am. Chem. Soc.* **2013** 135 18126.

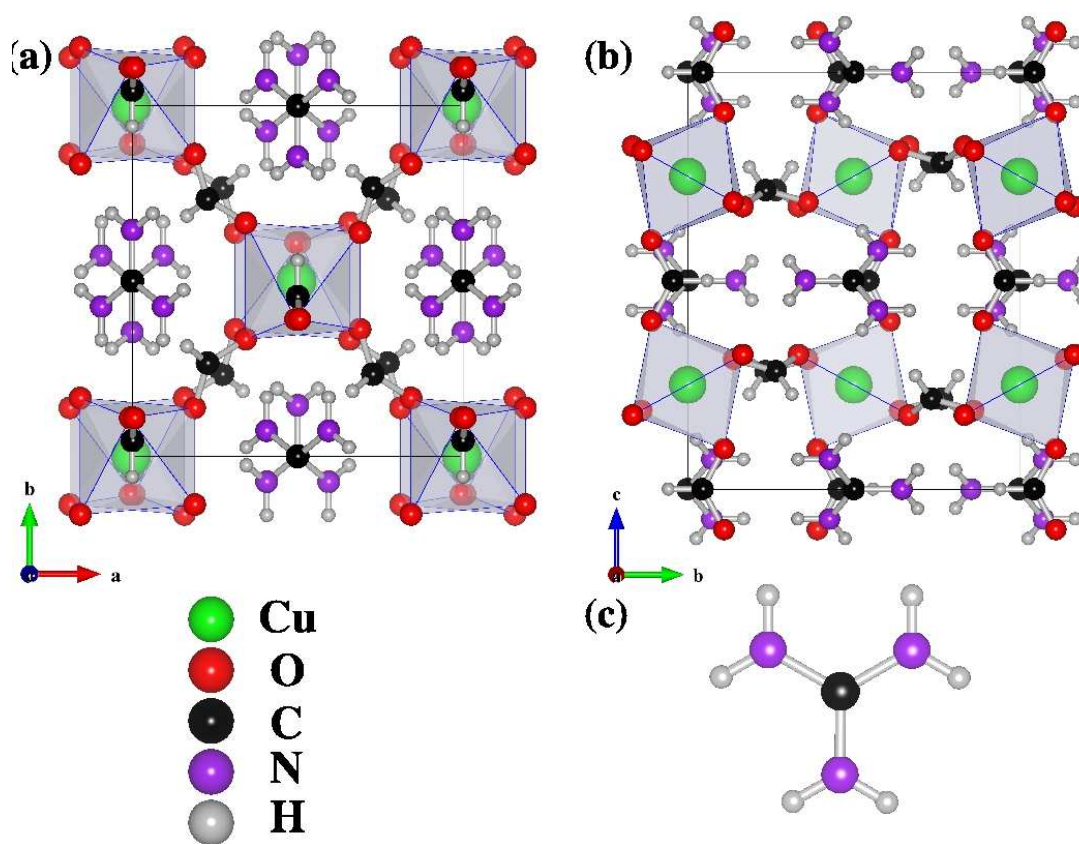


FIG. 1: (a) top and (b) side view of the crystalline unit cell; (c) Guanidinium cation.

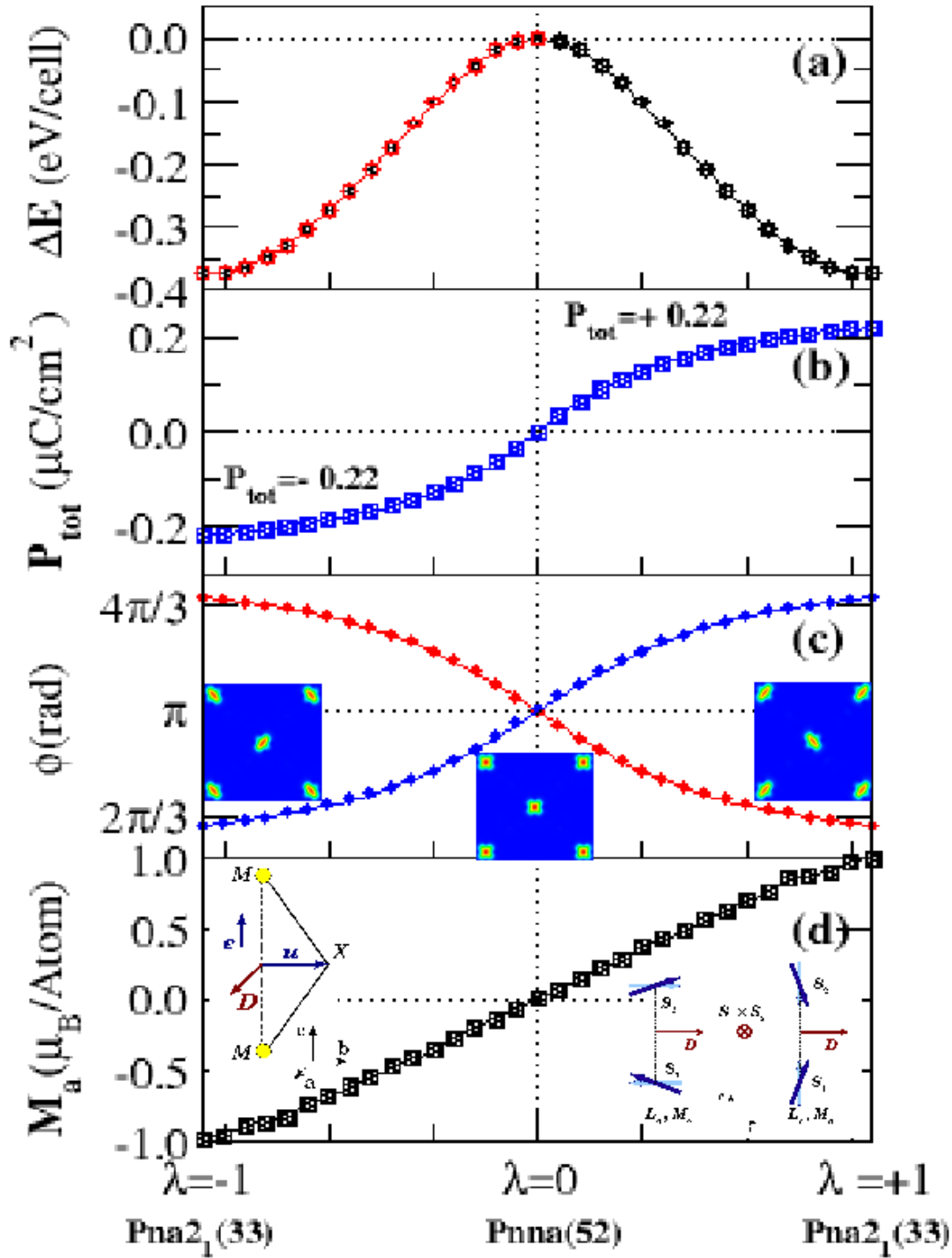


FIG. 2: (a) Variation of the total energy as a function of the structural distortion from the centric to the polar structures (switching path); (b) Ferroelectric polarization, (c) variation of the orbital ordering of the  $e_g$  electron and the JT  $\phi$  phase, (d) variation of the WFM component along the switching path; in (d), inset from the left: schematic view of the Dzyaloshinskii vector, defined as  $\mathbf{D}_c \propto \mathbf{u} \times \mathbf{e}$ , where  $\mathbf{u} \parallel b$  is the displacement vector of X ligand and  $\mathbf{e} \parallel c$  is the unit vector connecting neighboring spins belonging to different layers; inset from the right, symmetry-allowed WFM configurations shown, showing that spin chirality is always perpendicular to Dzyaloshinskii vector  $\mathbf{D}$ , resulting in no Dzyaloshinskii-Moriya interaction.

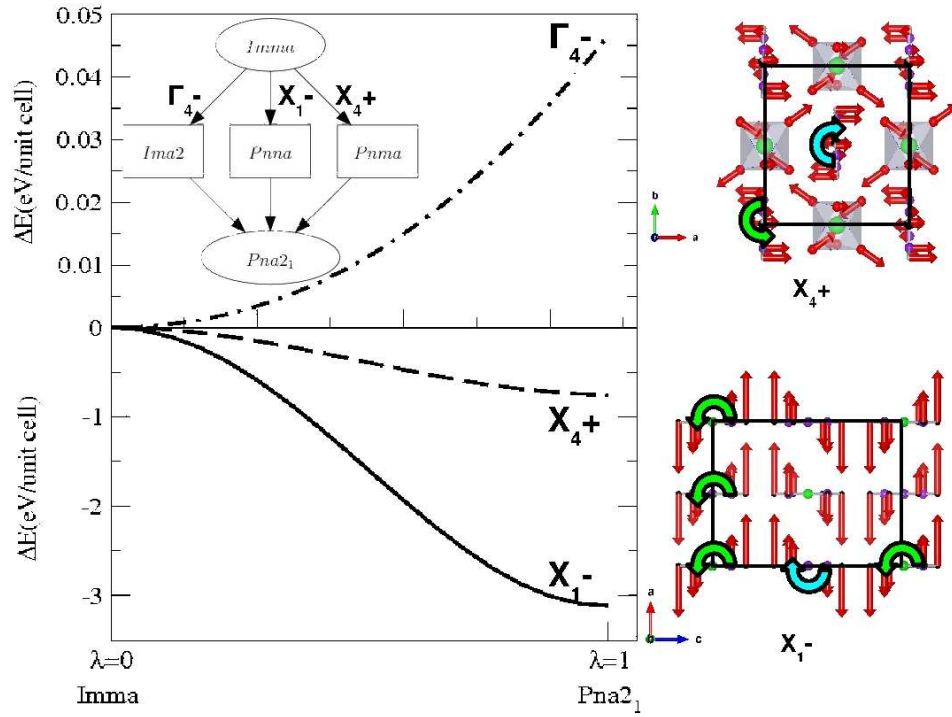


FIG. 3: Variation of the total energy as a function of the different distortion modes. In the inset, the group-subgroup tree is shown, having the  $Pna2_1$  as common maximal subgroup. In the right part of the figure, projected view of the the distortion modes associated to non-polar instabilities. The length of the arrows is proportional to the atomic displacements with respect to the  $Imma$  reference structure. The curved arrows denote clockwise or counterclockwise rotations.